Sci. Bull. (2015) 60(13):1157–1169
DOI 10.1007/s11434-015-0792-1

www.scibull.com
www.springer.com/scp

Review

Physics & Astronomy

Specially shaped Bessel-like self-accelerating beams along predesigned trajectories

Juanying Zhao · I. D. Chremmos · Ze Zhang · Yi Hu · Daohong Song · Peng Zhang · N. K. Efremidis · Zhigang Chen

Received: 13 April 2015 / Accepted: 12 May 2015 / Published online: 18 June 2015

Abstract Over the past several years, spatially shaped self-accelerating beams along different trajectories have been studied extensively. Due to their useful properties such as resistance to diffraction, self-healing, and self-bending even in free space, these beams have attracted great attention with many proposed applications. Interestingly, some of these beams could be designed with controllable spatial profiles and thus propagate along various desired trajectories such as parabolic, snake-like, hyperbolic, hyperbolic secant, three-dimensional spiraling, and even self-propelling trajectories. Experimentally, such beams are realized typically by using a spatial light modulator so as to imprint a desired phase distribution on a Gaussian-like input wave front propagating under paraxial or nonparaxial conditions. In this paper, we provide a brief overview of our recent work on specially shaped self-accelerating beams, including Bessel-like, breathing Bessel-like, and vortex Bessel-like beams. In addition, we propose and demonstrate a new type of dynamical Bessel-like beams that can exhibit not only self-accelerating but also self-propelling during propagation. Both theoretical and experimental results are presented along with a brief discussion of potential applications.

Keywords Airy beams · Bessel beams · Vortex beams · Nondiffracting beams · Self-accelerating · Self-healing

J. Zhao · Y. Hu · D. Song (✉) · Z. Chen (✉)
TEDA Applied Physics Institute and School of Physics, Nankai University, Tianjin 300457, China
e-mail: songdaohong@gmail.com

Z. Chen
e-mail: zhigang@sfsu.edu

J. Zhao
Science and Technology on Solid-State Laser Laboratory, North China Institute of Electronics Optics, Beijing 100015, China

J. Zhao · P. Zhang · Z. Chen
Department of Physics and Astronomy, San Francisco State University, San Francisco, CA 94132, USA

I. D. Chremmos
Max Planck Institute for the Science of Light, 91058 Erlangen, Germany

Z. Zhang
Academy of Opto-Electronics, Chinese Academy of Sciences, Beijing 100094, China

N. K. Efremidis
Department of Mathematics and Applied Mathematics, University of Crete, 70013 Heraklion, Crete, Greece

1 Introduction

In 1979, Berry and Balazs [1] theoretically predicted a self-accelerating wave solution for the free space Schrödinger equation in the context of quantum mechanics. Such an interesting wave packet, described mathematically by an Airy function, evolves in time without spreading while accelerating transversely along a parabolic trajectory. The acceleration (or self-bending) occurs in spite of the fact that the center of gravity of these truncated waves remains invariant in agreement with Ehrenfest's theorem. This accelerating behavior can persist over long distances until diffraction effects eventually take over and can be explained through the principle of equivalence [2], in which a stationary Airy wave packet associated with a quantum mechanical particle in a constant gravitational field can be perceived as accelerating

upwards by a free-falling observer. Unfortunately, this ideal Airy wave packet in quantum physics is supposed to carry infinite energy which makes it more like a theoretical elegance rather than a physically realizable entity. The interest in this field was revived in 2007, when Christodoulides and co-workers introduced the concept of Airy wave packets into optics by theoretically proposing and experimentally demonstrating the finite-energy self-accelerating optical Airy beams [3, 4]. Since then, the interest in such nonconventional self-accelerating beams has blossomed [5–7], gifted with the ability to resist diffraction while undergoing self-acceleration and self-healing, alongside with numerous proposed applications [7–16], including particle manipulation, curved plasma generation, bending surface plasmons and electrons, single molecule imaging, and light-sheet microscopy.

In the past several years, great efforts have been made to uncover new accelerating wave solutions. In particular, apart from the paraxial Airy beams [3–5], nonparaxial self-accelerating beams in general capable of following curved trajectories with large bending angles were also found directly for the Maxwell equations and demonstrated experimentally [17–20], followed by other types of nonparaxial accelerating beams such as Mathieu and Weber beams [21–23]. Unfortunately, most of these solutions cannot be used to design beams with arbitrary trajectories. The latter are most efficiently designed using ray optics and the concept of caustics [24]. It should be noted that accelerating beams based on ray caustics are usually characterized by highly asymmetric transverse intensity profiles (such as the Airy beams with one or two oscillating tails). An intriguing question arises naturally: can we design accelerating beams that propagate along arbitrary trajectories and yet have controllable and possibly symmetric transverse profiles (such as Bessel-like or donut-shaped beam profiles)?

Earlier works have showed that Bessel-like beam patterns can be delivered along sinusoidal [25] or spiraling trajectories [26]. An even earlier work suggested snaking beams made of the series cascade of the so-called sword beams [27]. These beams are formed by a different ray structure, named conical-interference ray structure, which sets them clearly apart from the optical caustic beams. Quite recently, we proposed and demonstrated the self-accelerating Bessel-like beams with arbitrary trajectories [28, 29]. Using the concept of conical superposition, angular momentum can also be loaded onto such beams resulting in accelerating vortex Bessel-like beams [30, 31]. Indeed, tremendous efforts have been made for shaping the light with various desired structures and properties [32–41], and these studies have fueled the research interest in beam synthesis and engineering as one of the interdisciplinary areas beyond optics and photonics.

In this paper, we provide a brief overview of our recent work on spatially shaped accelerating beams along arbitrary trajectories, including the self-accelerating Bessel-like beams (self-bending in transverse direction) with or without vorticity, self-breathing Bessel-like beams (with self-pulsating peak intensity along propagation direction), as well as nonparaxial (with large bending angles) Bessel-like beams [37]. In addition, we propose and demonstrate a new class of self-accelerating beams that can also undergo self-propelling (with multiple rotating intensity blades) during propagation. Based on the phase modulation and superposition method, the ability of designing various kinds of accelerating beams with arbitrary trajectories and symmetric transverse profile is illustrated. These spatially shaped dynamical beams are gifted with properties such as resistance to diffraction, capability of self-healing, controllable beam profiles and tunable trajectories, which make them particularly attractive for many applications.

2 Paraxial accelerating beams

Under the paraxial approximation, the propagation of an optical beam obeys the Fresnel diffraction integral:

$$u(X,Y,Z)=\frac{1}{2\pi \mathrm{i}Z}\iint u(x,y,0)\mathrm{e}^{\mathrm{i}\frac{(X-x)^2+(Y-y)^2}{2Z}}\mathrm{d}x\mathrm{d}y, \tag{1}$$

where $u(x,y,0)=\exp(-(x^2+y^2)/w^2)\exp(\mathrm{i}Q(x,y))$ is a phase-modulated input optical field with the transverse (X, Y; x, y) and longitudinal (Z) coordinates being scaled from real coordinate (x', y', z') by α and $k\alpha^2$, respectively. Here, w is the beam width, k is the wave number and α is an arbitrary length scale. The input phase pattern $Q(x, y)$ determines the ray trajectories in free space. These rays can be designed to create a focal curve ($f(Z)$, $g(Z)$, Z) and Bessel function profile, namely Bessel-like beam, as shown in Fig. 1. Specifically, any point on this curve is the apex of a conical ray bundle emanating from a circle on the input plane. The radius and the location of the center of this circle are determined by the formulas derived in Refs. [28, 29]. The center in particular is the point at which the tangent of the trajectory at ($f(Z)$, $g(Z)$, Z) intersects the input plane. This scenario is schematically plotted in Fig. 1a. In this context, if the input condition is obstructed along some of these circles, the main lobe at the corresponding distance will disappear. By removing input annuli (groups of these expanding circles) in a periodic fashion, energy periodically disappeared from the curved trajectory which exhibits a pulsating and breathing central lobe and a discrete curved focal line, namely breathing self-accelerating Bessel-like beam, as shown in Fig. 1b [32]. On the other hand, the rays from a circle at the input plane can also be given angular momentum to create hyperboloids (Fig. 1c) with a minimum waist (Fig. 1c) that guides along a

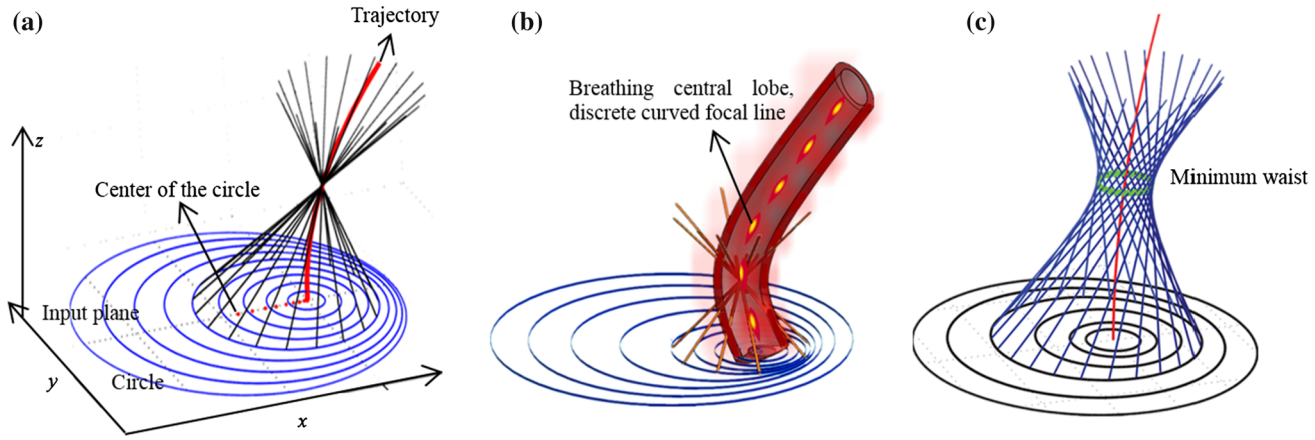

Fig. 1 (Color online) Schematic of the principle: Rays emitted from expanding circles on the input plane intersect on the specified focal curve. **a** A self-accelerating Bessel-like beam, where the dots are the shifting circle centers [28], **b** A breathing self-accelerating Bessel-like beam, where some circles are removed alternatingly so that the main lobe experiences breathing during propagation [32], **c** A self-accelerating vortex Bessel-like beam, where rays are skewed from each other rather than converging as in (**a**) and (**b**) [30]

predefined trajectory. In this way, vortex accelerating Bessel-like beams are produced [30, 31].

In the following sections, we will show that the transverse beam profiles generated via these schemes can be described approximated by the zero-order Bessel function $J_0(\beta r)$ (Fig. 1a, b) and higher-order Bessel function $J_m(\beta r)$ in polar coordinates (β is the normalized transverse wave number of the Bessel beam, $r = (\delta X^2 + \delta Y^2)^{1/2}$, and m is the order of vorticity in Fig. 1c), and they "focus" at controllable distances while keeping the beam structure remarkably invariant.

2.1 Self-accelerating Bessel-like beams along smooth trajectories

Let us start with some calculations for designing the accelerating Bessel-like beams, which are named so because the beam can bend along curved trajectories with a Bessel-like transverse beam profile. Note that the first partial derivatives of the phase Q satisfy $Q_x = (f - x)/Z$, $Q_y = (g - y)/Z$, where (x, y) marks the starting point of any ray in that conical ray bundle, as shown in Fig. 1a. The continuum of points $(x, y, 0)$ creates a geometric circle $C(Z)$ with center (x_0, y_0) and radius $R(Z)$ on $Z = 0$, which can be viewed as the isocurve of a function $Z(x, y)$. Since Q should be twice continuously differentiable, its mixed partials must be equal $Q_{xy} = Q_{yx}$, yielding $(x - x_0(Z))Z_y = (y - y_0(Z))Z_x$, where $x_0(Z) = f(Z) - Zf'(Z)$, $y_0(Z) = g(Z) - Zg'(Z)$. After some long algebraic procedure, the phase Q is shown to follow the formulas:

$$Q(x,y) = \frac{1}{2}\int_0^Z \left\{[f'(\zeta)]^2 + [g'(\zeta)]^2 - 1\right\} \mathrm{d}\zeta - \frac{(f-x)^2 + (g-y)^2}{2Z}, \tag{2}$$

$$Z^2 = [x - f(Z) + Zf'(Z)]^2 + [y - g(Z) + Zg'(Z)]^2. \tag{3}$$

The above algorithm is well defined only when Eq. (3) has a unique solution for Z, which is equivalent to the following inequality:

$$R'(Z) > Z\left[(f''(Z))^2 + (g''(Z))^2\right]^{1/2}. \tag{4}$$

Equation (4) defines the maximum propagation distance $Z_{\max}$ of the focal curve. Beyond $Z_{\max}$, a straight trajectory along its tangent direction is defined, so that the beam keeps a nondiffracting profile of a tilted standard Bessel beam. These Bessel-like beams inherit from standard ones the properties of diffractionless propagation and self-healing in addition to propagating along arbitrary trajectories. As examples, we have demonstrated parabolic, snake-like, hyperbolic as well as 3D spiraling trajectories [28, 29].

Figure 2 presents an example of the Bessel-like beam following the parabolic trajectory $((f(Z), g(z)) = (Z^2/40, 0))$. The phase structure shown in Fig. 2a is the one used to modulate a broad Gaussian input beam. We have numerically simulated the evolution of the wave using a split-step Fourier algorithm. The beam evolution recorded in the X–Z plane shows that the main peak follows a parabola up to 140 cm and a straight line thereafter (Fig. 2b). During acceleration, the transverse profiles (Fig. 2c–f) are recorded, which reveal a remarkably persistent main lobe (it is a very good fit to the function $J_0(r)$, although elongated along the axis of acceleration). Beyond $Z_{\max}$, acceleration stops and the symmetric Bessel profile is restored as our wave is essentially a tilted standard Bessel beam. And Eq. (1) can be rewritten as

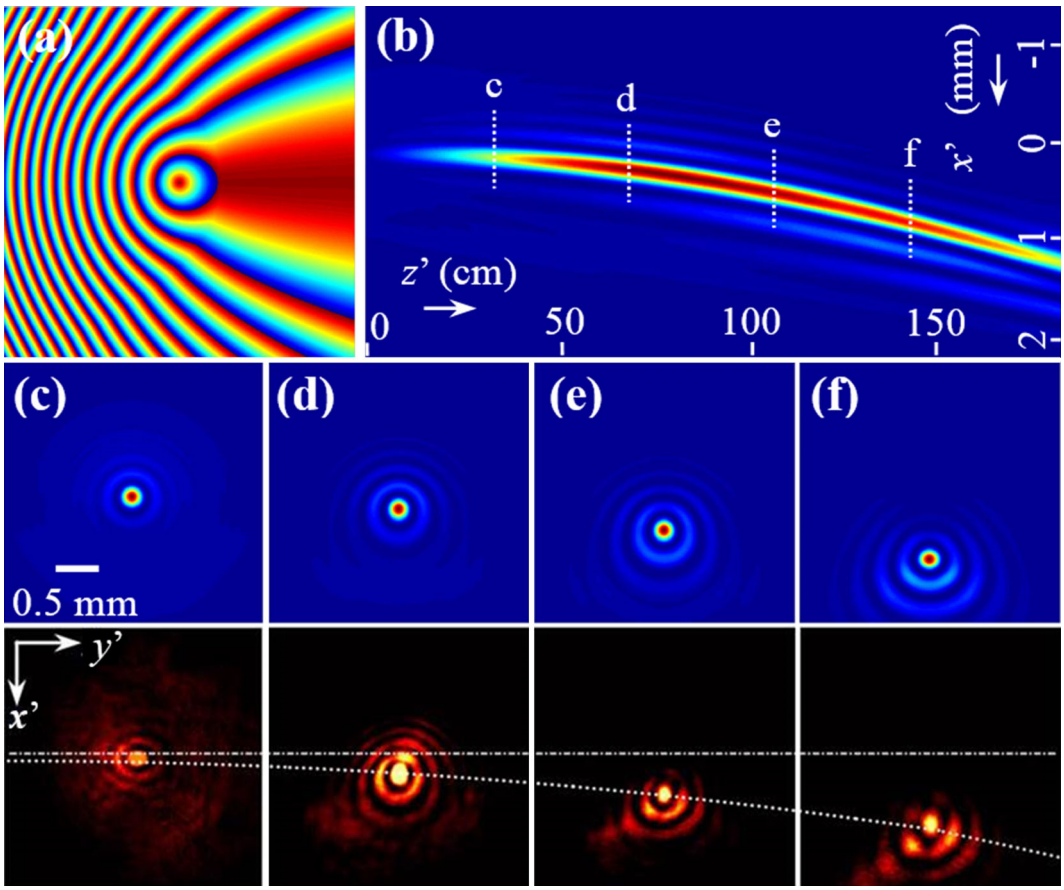

Fig. 2 (Color online) Numerical and experimental demonstrations of a self-accelerating Bessel-like beam along a parabolic trajectory. **a** Modulated input phase for the Bessel-like beam, **b** numerically simulated side-view propagation of the generated accelerating beam, **c**–**f** snapshots of numerical (middle row) and experimental (bottom row) transverse intensity patterns taken at different planes marked by the dashed lines in (**b**) [28, 29]

$$u(X, Y, Z) = J_0\left(\sqrt{(X-\eta Z)^2 + Y^2}\right) \times \exp\left(\mathrm{i}\eta X - \mathrm{i}(1+\eta^2)Z/2\right), \quad (5)$$

where J_0 is the Bessel function and η is a constant. Therefore, at any Z plane, the optical field around the focus behaves like a Bessel function modulated by a plane wave.

To experimentally realize such self-accelerating Bessel-like beams, we utilize computer-generated holography via a spatial light modulator (SLM) that is used to modulate the phase distribution of the input light field. A Gaussian beam emitted from an argon ion laser passes through the SLM programmed by a computer-generated hologram obtained by calculating the interference between the initial optical field and a tilted plane wave. Upon reflection from the hologram, the encoded beam information is reconstructed via a typical 4*f* system with spatial filtering. By shifting the CCD camera along z direction, we detect the images and record the movie at different propagation distances [29]. Figure 2c–f shows that the experimental results (bottom row) are in good agreement with numerical simulations (middle row). Using a similar approach, we have designed and demonstrated Bessel-like beams that propagate along several different types of trajectories, including sinusoidal, hyperbolic, and hyperbolic secant trajectories lying in a plane (2D trajectories) as well as spiraling trajectories in 3D space. In all cases, the observed trajectories agree well with the theoretical predictions. In addition, self-healing has also been demonstrated. In the latter work, the beam was partially blocked by an opaque wire thus losing its main lobe. During the subsequent propagation, the beam recovered its main lobe and restored its structure as expected [28, 29].

2.2 Breathing self-accelerating Bessel-like beams

As mentioned in the previous sections, a self-accelerating Bessel-like beam can be designed to exhibit a discrete (or breathing) curved trajectory by employing the scheme shown in Fig. 1b [32]. In this way, the intensity of the

central main lobe of these self-accelerating Bessel-like beams displays a pulsating or breathing feature, thus named "breathing self-accelerating Bessel-like beam". More specifically, the term "breathing" refers to that the central lobe of the beam disappears and reappears periodically as the energy of the beam alternately switches between the main lobe and the outer rings during propagation. These beams are produced by employing the initial condition $u(x,y,0)=\exp(-(x^2+y^2)/w^2)\exp(\mathrm{i}Q_1(x,y))$, where the phase Q_1 comes from a binarization of Q (the continuous phase of the Bessel-like beams), for instance:

$$Q_1=\begin{cases}0, & \min\_Q\le Q<\min\_Q+c,\\ 1, & \min\_Q+c\le Q<\min\_Q+2c,\\ 0, & \min\_Q+2c\le Q<\min\_Q+3c,\\ 1, & \min\_Q+3c\le Q<\min\_Q+4c,\\ \vdots & \vdots\\ \begin{cases}0, & 2[n/2]=n,\\ 1, & 2[n/2]\neq n,\end{cases} & \min\_Q+nc\le Q\le\max\_Q,\end{cases} \tag{6}$$

where max_Q and min_Q are the maximum and minimum values of Q, respectively, c is a constant satisfying the requirement $0<c<(\max\_Q-\min\_Q)/2$, the parameter $n=[\max\_Q/c]$ is the maximum integer of $\max\_Q/c$ and the square brackets are for integer conversion. After being modulated by the phase Q_1, the beam carrying a Bessel-like profile exhibits pulsation during propagation, as the peak intensity oscillates between the main lobe and the outer rings periodically.

Specifically, we obtain Q_1 from the following rules:

$$Q'=Q-2c\left[\frac{Q}{2c}\right],$$
$$Q_1=\begin{cases}1, & Q'\ge c,\\ 0, & Q'<c.\end{cases} \tag{7}$$

Figure 3 presents a typical example of the process used to produce Q_1. We start from a phase Q shown in Fig. 3a, which smoothly decreases along the radial direction. Then, Q is divided into a series of "periodic" rings Q' (Fig. 3b), which is the remainder of the Q when dividing by $2c$ ($c=\pi$). Here, the "period" $2c$ just means the modulated width ΔQ for each ring. Finally, a "well"-shaped phase Q_1 (Fig. 3c) is obtained from Q' by using Eq. (7). One can directly compare the phase structure between Q' and Q_1 in Fig. 3d, where the phase along the dotted line shown in Fig. 3b, c is plotted. With this phase Q_1, the beams created in $Z>0$ possess breathing transverse Bessel-like field patterns along a desired trajectory ($f(Z)$, $g(Z)$, Z) in free space.

The intuitive picture behind the evolution of the breathing beams is illustrated in Fig. 1b. Due to the "periodically" modulated phase Q_1, the interval of the breathing trajectory is determined by the annular width ΔQ at the input plane. The intensity peak alternately switches its location between the main lobe and the outer rings of the Bessel-like beam. As a typical example, we consider a beam propagating along a smooth hyperbolic trajectory in an oscillating configuration with a binary phase as shown in Fig. 4a. Figure 4b shows the numerical results of the breathing beam propagation. One can see that there are nine quasi-periodic breathings in the main lobe of the beam for the propagation distance of 200 cm. Indeed, the quasi-period of the breath can be controlled with ease by adjusting the modulation width c of the rings in the phase function Q_1. Transverse intensity patterns taken at different Z are shown in Fig. 4c–f, where it clearly illustrates that the beam possesses the Bessel-like intensity profile, and the location of peak intensity alternates between the central lobe and outer rings of the Bessel-like beam during propagation. It can be verified that these breathing Bessel-like beams also preserve their self-healing property.

Our detailed analysis shows that the pulsating feature of the peak intensity can also be introduced to the Bessel-like beams following other trajectories such as parabolic, hyperbolic secant, and 3D trajectories. These beams may be

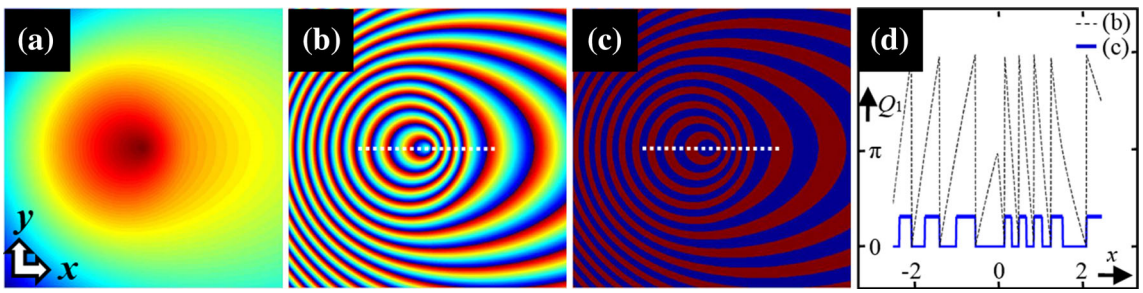

Fig. 3 (Color online) Phase structure for the generation of breathing accelerating beams as obtained from theoretical analysis. **a** The original phase Q obtained from Eq. (2), **b**, **c** the phase Q' and Q_1 obtained from Eq. (7), **d** plots of the phase Q_1 and Q' along the dotted lines in (**b**) and (**c**) [32]

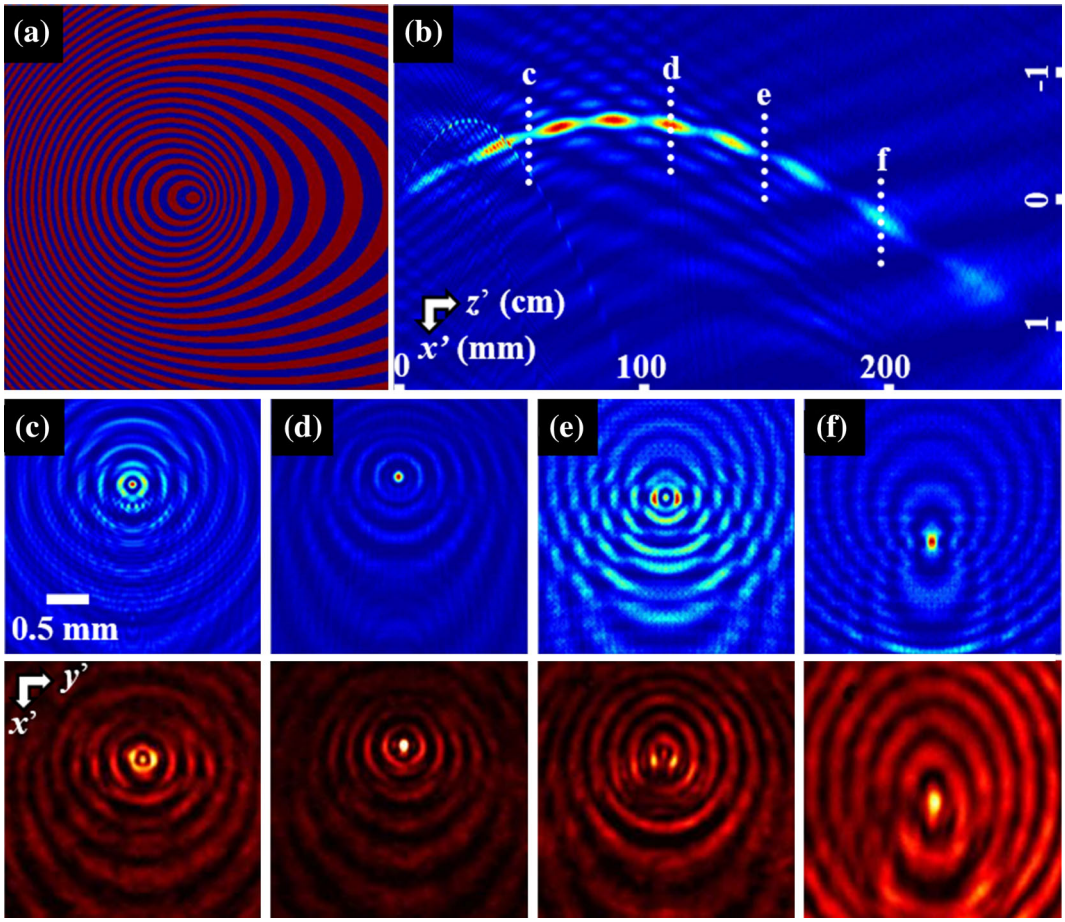

Fig. 4 (Color online) Numerical and experimental demonstrations of a breathing self-accelerating beam along a hyperbolic trajectory. **a** Binary-modulated input phase for the breathing self-accelerating beam with $f(Z) = \sqrt{0.64Z^2 - 32Z + 800} - \sqrt{800}$, $g(Z) = 0$, **b** numerically simulated side-view propagation of the generated beam, **c**–**f** numerical (middle row) and experimental (bottom row) snapshots of the transverse intensity patterns taken at different transverse planes marked by the dotted vertical lines in (**b**) [32]

particularly attractive for various applications including particle trapping and micromanipulation.

2.3 Vortex self-accelerating beams

Optical vortex beams, namely the beams that carry orbital angular momentum (OAM), have been an interesting subject of research for many decades [42–45]. These beams have a helical phase structure described as $\exp(im\theta)$, and m indicates the multiple of 2π round-trip phase around the vortex singularity, which is called the topological charge. Although attempts have been made to combine the properties of accelerating Airy beams and vortex beams, it remains a challenge to impose the OAM even onto the main lobe of a simple asymmetric 2D Airy beam [46]. Recently, we have proposed and demonstrated a new kind of self-accelerating beams carrying OAM in the form of accelerating vortex Bessel-like beams [30, 31]. These beams propagate along a desired trajectory ($f(Z)$, $g(Z)$, Z), having a profile that resembles a high-order Bessel function J_m with an invariant central dark core.

An accelerating vortex beam can be constructed using an approach similar to that developed in Ref. [28]. The initial beam profile is written in terms of a smooth amplitude function modulated by a helical phase Q_2 as $u(x, y, 0) = A(x, y)\exp(\mathrm{i}Q_2(x, y))$. Utilizing Eq. (1), we get

$$u(X, Y, Z) = \frac{1}{2\pi \mathrm{i} Z} \iint A(x, y) \times \exp\left[\mathrm{i}Q_2(x, y) + \mathrm{i}\frac{(X - x)^2 + (Y - y)^2}{2Z}\right] \mathrm{d}x\mathrm{d}y. \quad (8)$$

From this equation, the overall phase of the vortex beam is

$$\psi(X, Y) = Q_2(x, y) + \frac{(X - x)^2 + (Y - y)^2}{2Z}. \quad (9)$$

By applying the stationary phase method to the Fresnel integral, we obtain

$$\psi_X = \frac{X - x}{Z}, \quad \psi_Y = \frac{Y - y}{Z}. \tag{10}$$

Via the modulation of the phase ψ, the rays originating from a circle at the input plane lead to a vortex caustic at distance Z, which creates an oblique conical-like surface with a nonzero minimum waist (Fig. 1c).

As a typical example, we show in Fig. 5 the vortex beam with a topological charge $m = 3$ propagating along a hyperbolic trajectory. Following a similar algorithm to obtain the Bessel-like accelerating beams, the phase ψ can be solved as shown in Fig. 5a. The recorded trajectory of the dark core is in very good agreement with the theoretical prediction (Fig. 5b). The beam propagates along a hyperbolic curve and reaches a maximum intensity and the ultimate deviation at about 180 cm. The beam pattern looks similar to the higher-order Bessel beam J_3 profile with a central diffraction-free dark core (Fig. 5c–e), while the measured beam sizes at different propagation distances indicate that the main ring maintains almost a constant width during propagation. In addition, the topological charge remains unchanged even though the beam propagates along the curved trajectory. Such a dynamical optical beam combining features from the Bessel, Airy and vortex beams may provide a new tool for optical trapping and manipulation of microparticles when combined with optical tweezers technique [31].

2.4 Propelling self-accelerating beams

Optical propelling beams, namely the dynamical beams that exhibit multiple rotating intensity blades, have attracted great attention both due to their fundamental interest and due to their potential applications [47–51]. So far, a number of techniques have been proposed to create a rotating optical field intensity, including revolving mirrors [48, 52], interference of Laguerre-Gaussian modes [49, 50], rotating apertures [51], and the Moiré-pattern technique [53, 54]. Compared with previously developed methods,

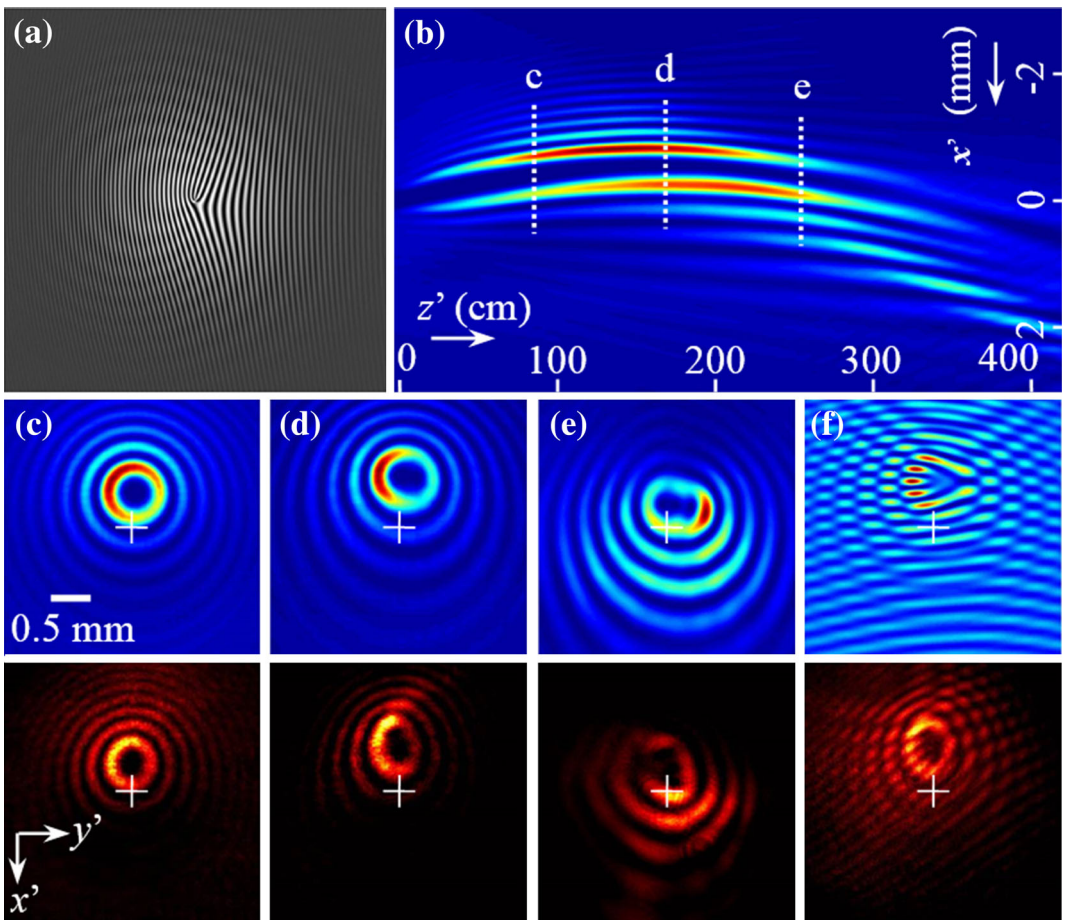

Fig. 5 (Color online) Numerical and experimental demonstrations of a triply charged vortex beam traveling along a hyperbolic trajectory. **a** Computer-generated hologram with desired phase information, **b** numerically simulated side-view propagation of the generated beam, **c**–**e** numerical (middle row) and experimental (bottom row) transverse beam patterns taken at different marked positions in (**b**), **f** interferograms from the pattern (**d**) with an inclined plane wave, showing the triply charged vorticity

the Moiré technique we developed recently has the advantage that all the rotation features of the beams can be changed at ease without any mechanical movement or phase-sensitive interference. It is also of great interest to introduce the propelling intensity into accelerating beams based on the Moiré technique. In this section, such propelling accelerating beams are created and analyzed theoretically and demonstrated experimentally. In theory, these beams are generated by overlapping a vortex accelerating beam and a plane wave, i.e., $u(x, y, 0) = u_1(x, y, 0) + u_2(x, y, 0)$, where $u_1(x, y, 0) = \exp(-(x^2 + y^2)/w^2)\exp(iQ_2(x, y))$ is a vortex accelerating beam and $u_2(x, y, 0) = \exp(ikx)$ is a plane wave.

To create the desired Moiré fringes, we overlap a moving straight-line grating (computer-generated hologram from two plane waves) and a fork-type grating with topological charge of $m = 3$ (the interference between a plane wave and a self-accelerating vortex beam), as shown in Fig. 6a–c. Based on the superposed gratings (Fig. 6d), Fig. 6e clearly illustrates that the generated beam propagates along a parabolic trajectory. Figure 6f–i shows numerically and experimentally retrieved transverse intensity

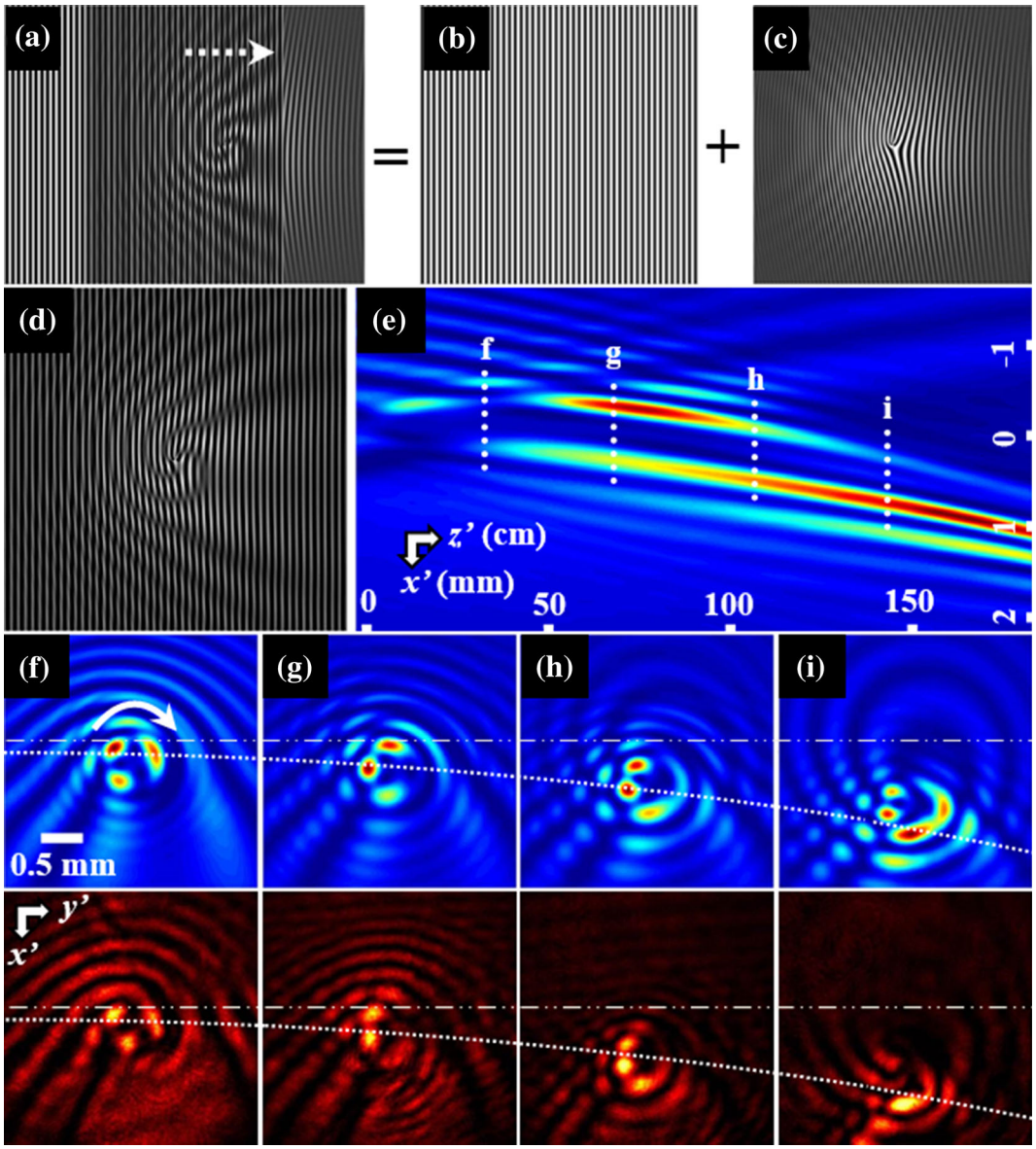

Fig. 6 (Color online) **a–d** The Moiré pattern used for generating a multiblade propelling accelerating beam formed by overlapping/translating a straight-line grating (**b**) with respect to a fork-type grating (**c**), where the fork-type grating is associated with a triply charged vortex, **e** numerically simulated side-view propagation of the propelling beam, **f–i** numerical (third row) and experimental (bottom row) transverse intensity patterns at different longitudinal positions marked in (**e**); the dashed arrow in (**a**) indicates the moving direction of the straight-line grating, and the solid arrow in (**f**) indicates the rotating direction of the dynamical beam pattern

patterns from the Moiré fringes of Fig. 6e at different longitudinal positions. From these figures, it is obvious that the beam profile consists of three intensity blades, with each blade rotating around the central dark core due to moving of the straight-line grating. In this scheme, the number of intensity blades is determined by the topological charge of the vortex. The rotation direction (marked by the white solid arrow) depends on the direction of the grating movement and the sign of the topological vortex charge, and the rotation speed is proportional to the speed of the grating motion. Overall, the Moiré pattern technique allows convenient changes of the number of intensity blades, as well as the rotation direction and speed of the intensity pattern. The generation of these propelling beams represents a transition from linear translation to rotation and from the vortex phase singularity to azimuthal intensity variation without using any mechanical rotating system.

Likewise, a propelling and accelerating beam can also propagate along different trajectories, as demonstrated theoretically and experimentally. Figure 7 illustrates typical experimental results of the generated propelling beams along a 3D trajectory ($f(Z) = 5\tanh[0.12(Z-10)] + 5$, $g(Z) = 6\,\mathrm{sech}[0.12(Z-10)]$). Figure 7a shows schematically that the reconstructed propelling beam from the Moiré technique propagates along the 3D trajectory. Figure 7b–d show numerical and experimental results of dynamical transverse intensity patterns obtained with this technique at different longitudinal positions. As seen from these results, the rotating beam profile is primarily composed of three rotating blades. These propelling beams bring about the possibility for dynamic microparticle manipulation based on the Moiré technique which is inherently immune to environmental perturbations. These fine-shaped dynamical light beams may also find applications in micromachining and in developing multifunctional rotating optical tweezers for biological research.

3 Nonparaxial self-accelerating Bessel-like beams

In this section, we discuss briefly Bessel-like beams beyond the paraxial approximation [37]. Nonparaxiality plays an important role when the transverse oscillations of a beam are in a scale comparable to or smaller than the operating wavelength. Under this condition, the wave evolution is governed by the vector Helmholtz equation:

$$(\nabla^2 + k^2)\boldsymbol{E} = \boldsymbol{0}. \tag{11}$$

According to which, the wave vector components satisfy the dispersion relation $k_z = (k^2 - k_x^2 - k_y^2)^{1/2}$. For a given input condition, the Helmholtz equation is solved by the

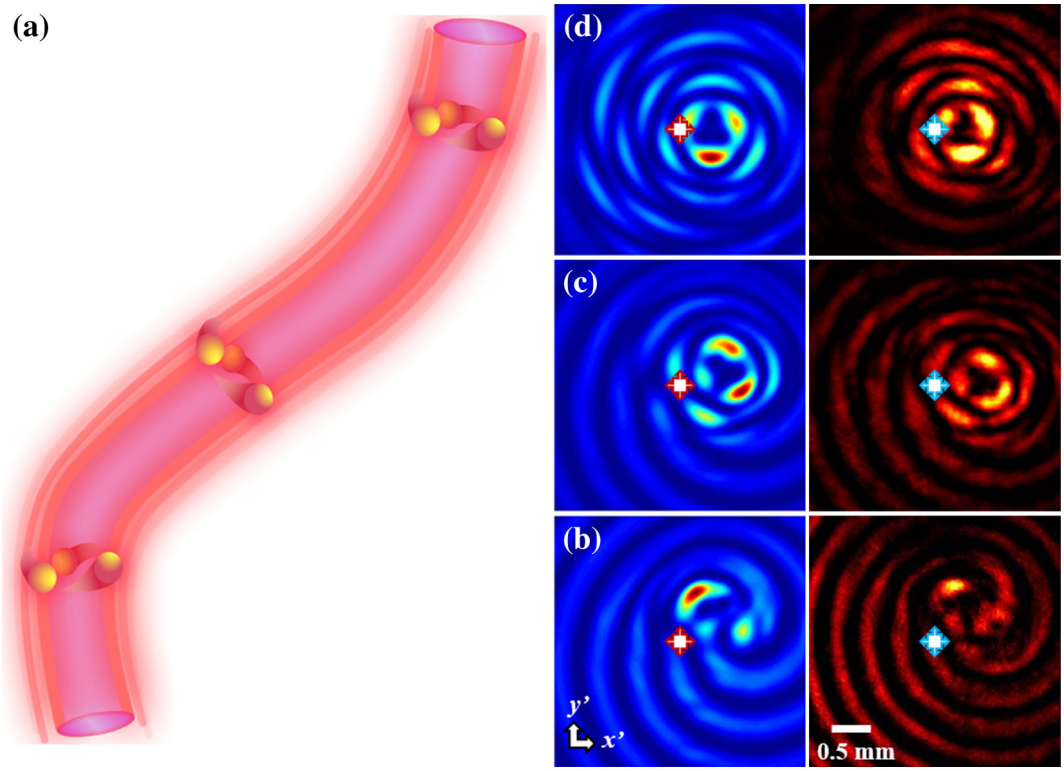

Fig. 7 (Color online) The three-blade propelling accelerating beam propagates along a 3D trajectory. **a** Schematic of the beam propagation, **b–d** numerical (middle column) and experimental (right column) transverse intensity patterns taken at different propagation distances as illustrated in (**a**)

Rayleigh–Sommerfeld formula for one component of the electric field vector potential

$$u(\boldsymbol{R}) = -\frac{k^3 Z}{2\pi}\iint u(\boldsymbol{r})G(k|\boldsymbol{R}-\boldsymbol{r}|)\mathrm{e}^{\mathrm{i}k|\boldsymbol{R}-\boldsymbol{r}|}\mathrm{d}\boldsymbol{r}, \tag{12}$$

where we assume the input to be formulated by a slowly varying envelope times a phase factor, i.e., $u(\boldsymbol{r}) = U(\boldsymbol{r})\mathrm{e}^{\mathrm{i}Q_3(r)}$, $G(r) = \mathrm{i}r^{-2} - r^{-3}$ is the Green's function, $\boldsymbol{R} = (X, Y, Z)$ is the observation position, and $\boldsymbol{r} = (x, y, 0)$ spans the input plane.

By modulating the input light field with the phase Q_3, the rays create a continuous focal line in the free space with a given parametric trajectory $\boldsymbol{F}(Z) = (f(Z), g(Z), Z)$. At any point on this line, rays emanating from a geometric locus in the input plane intersect and interfere to create a Bessel-like profile. Therefore, one can realize a Bessel-like beam following the pre-designed trajectories through employing the phase modulation shown below at the input plane

$$(Q_{3x}, Q_{3y}) = \frac{k}{|\boldsymbol{F}(Z)-\boldsymbol{r}|}(f(Z)-x, g(Z)-y). \tag{13}$$

For the trajectory $(f(Z), 0)$, here $g(Z) = 0$, Fig. 8 shows the ray-optics schematic for the diffraction of the potential function $u(\boldsymbol{r})$. Rays emitted from expanding ellipses interfere to create a curved focal line (the curve trajectory).

Using the concept of auxiliary vector potentials, the electromagnetic problem of a vectorial Bessel-like beam in the nonparaxial region can be reduced to the dynamics of a scalar wave function (a single component of a vector potential) according to the above diffraction integral. Again, the phase Q_3 satisfies $Q_{3xy} = Q_{3yx}$, from which we can obtain

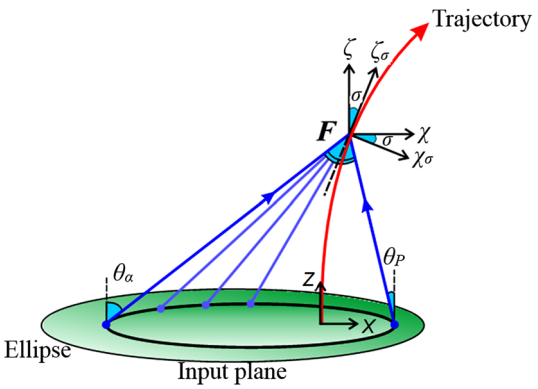

Fig. 8 (Color online) Ray-optics schematic for the diffraction of the potential function $u(\boldsymbol{r})$. Shown on the $Y = 0$ plane are the global coordinates X, Z, and at the focal point the local coordinates χ, ζ [37]

$$Z_{xy}\left(x - f - \frac{Z}{f'}\right) = -Z_y\left[y^2 + \frac{Z}{f'}(x-f) + Z^2\right]. \tag{14}$$

The shape of the ellipse satisfies the following equation:

$$\frac{(x-x_0)^2}{a^2} + \frac{y^2}{b^2} = 1, \tag{15}$$

where $a(Z) = Z[(\omega-1)(1+\omega f'^2)]^{1/2}$, $b(Z) = Z(\omega-1)^{1/2}$, $x_0(Z) = f - \omega Z f'$, and $\omega(Z)$ is an arbitrary dimensionless function.

After some analyses, the phase at any point $\boldsymbol{r}$ on input plane is given by $Q_3(\boldsymbol{r}) = P(Z) - k|\boldsymbol{R}-\boldsymbol{r}|$, where Z corresponds to the elliptical locus $C(Z)$ passing from this point, $P(Z) = k\int_0^Z \frac{\cos[\gamma(z)]}{\cos[\sigma(z)]}\mathrm{d}z$, $\mathrm{d}z/\cos\sigma = \mathrm{d}z(1+f'^2)^{1/2}$, and the cone half angle $\gamma = \arctan\left(\frac{\omega-1}{1+\omega f'^2}\right)^{1/2}$, which describes the width of the beam's main lobe. Providing that the input amplitude satisfies $U = (2\pi k_\perp \rho_\sigma)^{-1/2}\mathrm{e}^{\mathrm{i}\pi/4}$ (where $k_\perp = k\sin\gamma$ and ρ_σ is the distance from the axis of the beam), the beam evolution can be expressed as

$$u(\boldsymbol{F} + \delta\boldsymbol{R}_\sigma) \approx J_0(k_\perp\rho_\sigma)\exp\left[\mathrm{i}k_\parallel\left(\frac{Z}{\cos\sigma} + \zeta_\sigma\right)\right], \tag{16}$$

where $k_\parallel = k\cos\gamma$. Equation (16) clearly represents an ideal diffraction-free Bessel beam that propagates with wave vector $k_\parallel$. Therefore, the ray-optics approximation is consistent with the fact that the Helmholtz equation supports the Bessel beam solutions.

As an example, the Bessel-like beam is designed to propagate again along a parabolic trajectory. In the simulations shown in Fig. 9, we adopt the trajectory function $(f(Z), g(Z)) = (0.015Z^2, 0)$ and parameter $\gamma = 30°$; here, all distances are measured in wavelengths. For a standard nonaccelerating Bessel beam, the corresponding subwavelength FWHM of the central lobe can be obtained with γ value. By employing the phase structure presented in Fig. 9a, a fully vectorial nonparaxial accelerating Bessel-like wave is obtained whose intensity follows a parabolic trajectory (Fig. 9b–g). Note that the trajectory of the simulated beam agrees well with the predesigned one. In Fig. 9e, the longitudinal component E_Z is initially weak, but its magnitude increases to become comparable to the transverse component E_X as the trajectory of the beam gets more inclined. This is because the more the wave loses its transverse nature, the more it departs from the paraxial regime. For the total electric energy density (Fig. 9g), one sees that the overall beam profile inherits the expected Bessel-like form with familiar ring structure (elongated along the direction of acceleration). And the presence of the longitudinal component does not affect the Bessel profile significantly.

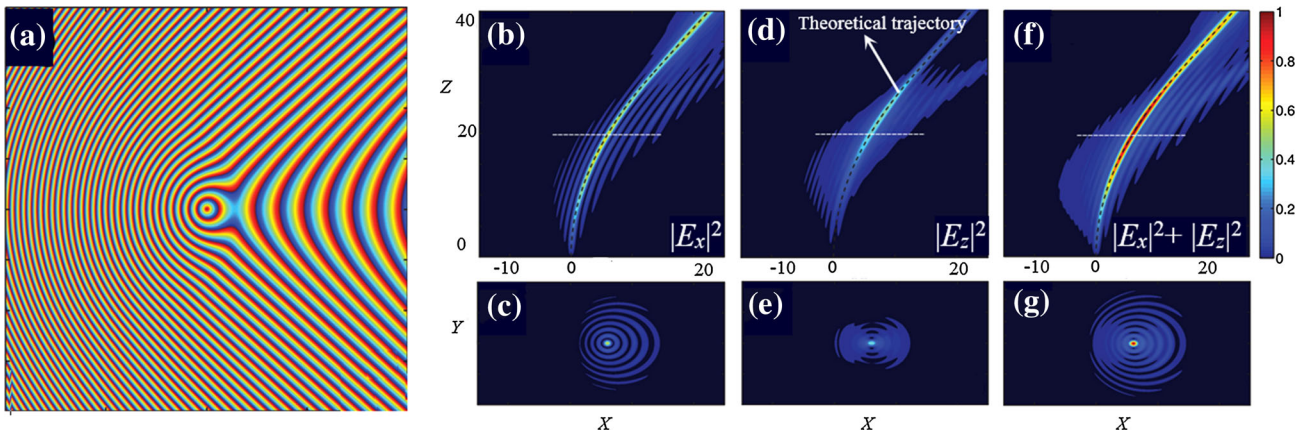

Fig. 9 (Color online) Simulation results for a nonparaxial accelerating Bessel-like beam with a parabolic trajectory. **a** Input phase structure, **b** evolution of $|E_X|^2$ on the plane $Y = 0$, and **c** its transverse profile on the plane $Z = 20$ as marked in (**b**) with a white dashed line, **d**–**e** the same for $|E_Z|^2$. **f**–**g** The same for the electric energy density $|E_X|^2 + |E_Z|^2$. **b**, **d**, **f** The black dashed curves in the beam center lobe indicate the theoretical trajectory. The maps have the same color code to allow direct comparison [37]

In brief, the fully vectorial nonparaxial accelerating Bessel-like waves have been demonstrated by an appropriate modification of the conical ray pattern of the standard Bessel beams. We have found that these numerical results are in good agreement with theoretical design, in cases of parabolic, hyperbolic, hyperbolic secant, and 3D trajectories. In contrast to caustic-based beams which are highly asymmetric in their transverse intensity distribution, these new accelerating beams provide the convenience of a symmetric Bessel-like intensity profile which is much needed for many applications.

4 Potential applications

All of the beams discussed above, which possess nearly symmetric transverse beam profiles together with features of nondiffracting, self-healing, and tunable trajectories, may be particularly attractive for various applications already proposed [7–16], including optical microparticles manipulation, generation of special light bullets, generation of curved plasma channels, routing of surface plasmon polaritons, generation of self-bending electron beams without any external field, and high-resolution imaging and microscopy. These promising applications have further advanced the research of self-accelerating beams and beam shaping in general in the fields beyond optics and photonics.

Optical manipulation of particles with lasers is an indispensable tool across many branches of science, including molecular biology, medicine, nanotechnology, atmospheric science and colloidal physics. In this field, the leading tools are optical tweezers with specially shaped beam profiles, which apply gradient forces and radiation pressure on trapped transparent particles. With Bessel-like profile, these beams can trap the micro-objects into the central area of the beams and transport them to the desired destination along predesigned curved route, promising for long-range material transport. As an "optical wrench", the self-propelling beams are suitable for particle grouping and rotation owing to their dynamical intensity blades. Meanwhile, rotation of trapped particles offers another important degree of freedom for optical manipulation, promising for applications in biotechnology.

In atmospheric sciences, these beams possessing high transmission efficiency and self-healing properties are desirable for light propagation through the atmospheric turbulence or other complex scattering media. Meanwhile, with the self-accelerating property, these beams can be used to generate curved plasma channels and even to control electric discharges.

5 Summary

In this paper, we have reviewed briefly the conception and development of dynamical spatially shaped Bessel-like accelerating beams with a central symmetric transverse intensity profile traveling along arbitrary trajectories. Based on our design, the self-accelerating Bessel-like beams, breathing Bessel-like beams and vortex Bessel-like beams have all been demonstrated. In addition, we have shown that it is feasible to create self-propelling while simultaneously self-accelerating optical beams by the use of the phase design combined with the Moiré technique. Finally, such specially designed accelerating beams might be synthesized beyond the paraxial region based on the ray-optics interpretation of the rigorous Rayleigh–Sommerfeld diffraction formula. Our results may lead to new possibilities for optical beam shaping and beam engineering that may find a variety of potential applications, while continued research on accelerating beams keeps bringing up new

momentum to the arena of optical beam shaping and applications [55–64].

Acknowledgments This work was supported by the National Natural Science Foundation of China (61475161 and 11304165), China Scholarship Council, and Natural Science Foundation (NSF) and Air Force Office of Scientific Research (AFOSR) in USA.

Conflict of interest The authors declare that they have no conflict of interest.

References

1. Berry MV, Balazs NL (1979) Nonspreading wave packets. Am J Phys 47:264–267
2. Greenberger DM (1980) Comment on "Nonspreading wave packets". Am J Phys 48:256
3. Siviloglou GA, Christodoulides DN (2007) Accelerating finite energy Airy beams. Opt Lett 32:979–981
4. Siviloglou GA, Broky J, Dogariu A et al (2007) Observation of accelerating Airy beams. Phys Rev Lett 99:213901
5. Hu Y, Siviloglou GA, Zhang P et al (2012) Self-accelerating Airy beams: generation, control, and applications. In: Chen Z, Morandotti R (eds) Nonlinear photonics and novel optical phenomena. Springer, New York, pp 1–46
6. Bandres MA, Kaminer I, Mills M et al (2013) Accelerating optical beams. Opt Photonics News 24:30–37
7. Zhang Z, Hu Y, Zhao JY et al (2013) Research progress and application prospect of Airy beams. Chin Sci Bull 58:3513–3520 (in Chinese)
8. Baumgartl J, Mazilu M, Dholakia K (2008) Optically mediated particle clearing using Airy wavepackets. Nat Photonics 2:675–678
9. Zhang P, Zhang Z, Prakash J et al (2011) Trapping and guiding microparticles with morphing autofocusing Airy beams. Opt Lett 36:2883–2885
10. Polynkin P, Kolesik M, Moloney JV et al (2009) Curved plasma channel generation using ultraintense Airy beams. Science 324:229–232
11. Zhang P, Wang S, Liu Y et al (2011) Plasmonic Airy beams with dynamically controlled trajectories. Opt Lett 36:3191–3193
12. Minovich A, Klein AE, Janunts N et al (2011) Generation and near-field imaging of Airy surface plasmons. Phys Rev Lett 107:116802
13. Li L, Li T, Wang SM et al (2011) Plasmonic Airy beam generated by in-plane diffraction. Phys Rev Lett 107:126804
14. Voloch-Bloch N, Lereah Y, Lilach Y et al (2013) Generation of electron Airy beams. Nature 494:331–335
15. Jia S, Vaughan JC, Zhuang X (2014) Isotropic three-dimensional super-resolution imaging with a self-bending point spread function. Nat Photon 8:302–306
16. Vettenburg T, Dalgarno HI, Nylk J et al (2014) Light-sheet microscopy using an Airy beam. Nat Methods 5:541–544
17. Kaminer I, Bekenstein R, Nemirovsky J et al (2012) Nondiffracting accelerating wave packets of Maxwell's equations. Phys Rev Lett 108:163901
18. Courvoisier F, Mathis A, Froehly L et al (2012) Sending femtosecond pulses in circles: highly nonparaxial accelerating beams. Opt Lett 37:1736–1738
19. Zhang P, Hu Y, Cannan D et al (2012) Generation of linear and nonlinear nonparaxial accelerating beams. Opt Lett 37:2820–2822
20. Aleahmad P, Miri MA, Mills MS et al (2012) Fully vectorial accelerating diffraction-free Helmholtz beams. Phys Rev Lett 109:203902
21. Zhang P, Hu Y, Li T et al (2012) Nonparaxial Mathieu and Weber accelerating beams. Phys Rev Lett 109:193901
22. Bandres MA, Rodriguez-Lara BM (2013) Nondiffracting accelerating waves: weber waves and parabolic momentum. New J Phys 15:013054
23. Libster-Hershko A, Epstein I, Arie A (2014) Rapidly accelerating Mathieu and Weber surface plasmon beams. Phys Rev Lett 113:123902
24. Mathis A, Courvoisier F, Giust R et al (2013) Arbitrary nonparaxial accelerating periodic beams and spherical shaping of light. Opt Lett 38:2218–2220
25. Morris JE, Cizmár T, Dalgarno HIC et al (2010) Realization of curved Bessel beams: propagation around obstructions. J Opt 12:124002
26. Jarutis V, Matijosius A, Trapani PD et al (2009) Spiraling zero-order Bessel beam. Opt Lett 34:2129–2131
27. Rosen J, Yariv A (1995) Snake beam: a paraxial arbitrary focal line. Opt Lett 20:2042–2044
28. Chremmos ID, Chen Z, Christodoulides DN et al (2012) Bessel-like optical beams with arbitrary trajectories. Opt Lett 37:5003–5005
29. Zhao J, Zhang P, Deng D et al (2013) Observation of self-accelerating Bessel-like optical beams along arbitrary trajectories. Opt Lett 38:498–500
30. Chremmos ID, Zhao JY, Christodoulides DN et al (2014) Diffraction-resisting vortex Bessel beams with arbitrary trajectories. In: Conference on lasers and electro-optics: quantum electronics and laser science (QELS_fundamental science), Optical Society of America Technical Digest (online), San Jose, CA USA, p FM3D.1
31. Zhao JY, Zhang P, Liu JJ et al (2013) Trapping and guiding microparticles with self-accelerating vortex beams. In: Conference on lasers and electro-optics: science and innovations, Optical Society of America Technical Digest (online), San Jose, CA USA, p CM1 M.6
32. Zhao JY, Zhang P, Deng D et al (2013) Self-accelerating and self-breathing Bessel-like beams along arbitrary trajectories. Chin Opt Lett 11:110701
33. Deng HC, Yuan LB (2013) Two-dimensional Airy-like beam generation by coupling waveguides. J Opt Soc Am A: 30:1404–1408
34. Jiang YF, Huang KK, Lu XH (2012) Airy-related beam generated from flat-topped Gaussian beams. J Opt Soc Am A: 29:1412–1416
35. Zhang YQ, Belić MR, Zheng HB et al (2013) Fresnel diffraction patterns as accelerating beams. Europhys Lett 104:34007
36. Zhang YQ, Belić MR, Zheng HB et al (2014) Three-dimensional nonparaxial accelerating beams from the transverse Whittaker integral. Europhys Lett 107:34001
37. Chremmos ID, Efremidis NK (2013) Nonparaxial accelerating Bessel-like beams. Phys Rev A 88:063816
38. Ren ZJ, Wu Q, Shi YL et al (2014) Production of accelerating quad Airy beams and their optical characteristics. Opt Express 22:15154–15164
39. Hu Y, Bongiovanni D, Chen ZG et al (2013) Periodic self-accelerating beams by combined phase and amplitude modulation in the Fourier space. Opt Lett 38:3387–3389
40. Efremidis NK, Christodoulides DN (2010) Abruptly autofocusing waves. Opt Lett 35:4045–4047
41. Chremmos I, Efremidis NK, Christodoulides DN (2011) Pre-engineered abruptly autofocusing beams. Opt Lett 36:1890–1892
42. Allen L, Beijersbergen MW, Spreeuw RJC et al (1992) Orbital angular momentum of light and the transformation of Laguerre-Gaussian laser modes. Phys Rev A 45:8185–8189
43. Zhou GQ, Wang XG, Dai CQ et al (2014) Angular momentum density of a Gaussian vortex beam. Sci China Phys Mech Astron 57:619–627

44. Zhou GQ, Cai YJ, Dai CQ (2013) Hollow vortex Gaussian beams. Sci China Phys Mech Astron 56:896–903
45. Zhou GQ, Wang XG, Chu XX (2013) Fractional Fourier transform of Lorentz–Gauss vortex beams. Sci China Phys Mech Astron 56:1487–1494
46. Dai HT, Liu YJ, Luo D et al (2010) Propagation dynamics of an optical vortex imposed on an Airy beam. Opt Lett 35:4075–4077
47. O'Neil AT, Padgett MJ (2002) Rotational control within optical tweezers by use of a rotating aperture. Opt Lett 27:743–745
48. Madison KW, Chevy F, Wohlleben W et al (2000) Vortex formation in a stirred Bose–Einstein condensate. Phys Rev Lett 84:806–809
49. Sasaki K, Koshioka M, Misawa H et al (1992) Optical trapping of a metal particle and a water droplet by a scanning laser beam. Appl Phys Lett 60:807–809
50. Paterson L, MacDonald MP, Arlt J et al (2001) Controlled rotation of optically trapped microscopic particles. Science 292:912–914
51. Rotschild C, Saraf M, Barak A et al (2008) Complex nonlinear opto-fluidity. In: Frontiers in optics, Optical Society of America Technical Digest (CD), Rochester, USA, p FME2
52. Anastassiou C, Pigier C, Segev MC et al (2001) Self-trapping of bright rings. Opt Lett 26:911–913
53. Zhang P, Huang S, Hu Y et al (2010) Generation and nonlinear self-trapping of optical propelling beams. Opt Lett 35:3129–3131
54. Zhang P, Hernandez D, Cannan D et al (2012) Trapping and rotating microparticles and bacteria with moiré-based optical propelling beams. Biomed Opt Express 3:1891–1897
55. Deng D, Gao Y, Zhao J et al (2013) Three-dimensional nonparaxial beams in parabolic rotational coordinates. Opt Lett 38:3934–3936
56. Gong L, Ren YX, Xue GS et al (2013) Generation of nondiffracting Bessel beam using digital micromirror device. Appl Opt 52:4566–4575
57. Ornigotti M, Aiello A (2014) Generalized Bessel beams with two indices. Opt Lett 39:5618–5621
58. Wang F, Zhao C, Dong Y et al (2014) Generation and tight-focusing properties of cylindrical vector circular Airy beams. Appl Phys B 117:905–913
59. Zhu WG, She WL (2014) Improved nonparaxial accelerating beams due to additional off-axis spiral phases. J Opt Soc Am A 31:2365–2369
60. Liu ZH, Zhang YX, Zhang Y et al (2014) All-fiber self-accelerating Bessel-like beam generator and its application. Opt Lett 39:6185–6188
61. Huang C, Lu H (2014) Accelerating propagation properties of misplaced Hermite–Gaussian beams. J Opt Soc Am A 31:1762–1765
62. Liu X, Zhao D (2014) Optical trapping Rayleigh particles by using focused multi-Gaussian Schell-model beams. Appl Opt 53:3976–3981
63. Vetter C, Eichelkraut T, Ornigotti M et al (2014) Generalized radially self-accelerating Helicon beams. Phys Rev Lett 113:183901
64. Schley R, Kaminer I, Greenfield E et al (2014) Loss-proof self-accelerating beams and their use in non-paraxial manipulation of particles' trajectories. Nat Commun 5:5189